# PRESENT UNDERSTANDING OF ELECTRON CLOUD EFFECTS IN THE LARGE HADRON COLLIDER

G. Arduini, V. Baglin, E. Benedetto, R. Cimino, P. Collier, I. Collins, K. Cornelis, B. Henrist, N. Hilleret, B. Jenninger, M. Jimenez, A. Rossi, F. Ruggiero, G. Rumolo*, D. Schulte, F. Zimmermann, CERN, Geneva, Switzerland

## Abstract

We discuss the predicted electron cloud build up in the arcs and the long straight sections of the LHC, and its possible consequences on heat load, beam stability, long-term emittance preservation, and vacuum. Our predictions are based on computer simulations and analytical estimates, parts of which have been benchmarked against experimental observations at the SPS.

## 1 INTRODUCTION

An electron cloud and its effects are observed in the CERN SPS, when operated with LHC-type beams. The electrons are created by a beam-induced multipacting process [1]. A similar electron build up in the LHC might complicate its commissioning and early operation. Simulations for the LHC can be benchmarked against SPS measurements.

## 2 INSTABILITIES

Instabilities due to electron cloud have been seen in the SPS with the LHC beam since 1999 [2, 3]. In the horizontal plane, we observe a coupled-bunch instability, whose wave length is comparable to the length of a 72-bunch train (called 'batch'). The growth time is about 1 ms (50 turns) and nearly independent of the bunch population. We believe that the coupled bunch wake in the horizontal plane is caused by the spatial structure of the electron cloud, which is concentrated in the form of two vertical stripes on either side of the beam, slowly following the beam motion. The coherent and incoherent components of the flat-chamber impedance can add to the electron-cloud wake [4]. In the vertical plane a single-bunch instability is observed. Its growth time is about 2 ms (100 turns) at the nominal LHC intensity, and it changes strongly with beam current. Countermeasures that were taken include the transverse damper system, which acts against the coupled-bunch instablity, and a high chromaticity, up to 20 units, suppressing the single-bunch effect. Most successful, however, was a dedicated 10-day scrubbing run in 2002, initially accompanied by an extensive electron-cloud activity and a high vacuum pressure, in the course of which the secondary emission yield of the vacuum chamber decreased substantially. However, at the end of the scrubbing run, the electron-cloud threshold was still about 20% lower than the nominal LHC intensity.

We can translate these observations to the LHC, by applying simplified scaling laws. The growth rate for the coupled bunch instability is roughly approximated by [5] $1/\tau \approx 2\pi r_p \beta c \rho_{el}/\gamma$. Taking an SPS beta function of

---

$\beta_{SPS} \approx 40$ m and a beam momentum of $p_{SPS} \approx 26$ GeV/c, the 1 ms growth time at injection into the SPS corresponds to an average electron density of $\rho_{el} \approx 3 \times 10^{11}$ m$^{-3}$. Assuming the same value of $\rho_{el}$, $\beta_{LHC} \approx 100$ m, and $p_{LHC} \approx 450$ GeV/c, at injection into the LHC the growth time would be 5 ms (50 turns). This number is comparable to the LHC feedback damping time. The TMCI-like single-bunch instability has a threshold [6]

$$N_{b,thr} \approx \frac{\gamma Q_s h_x h_y}{\beta C} \frac{2L_{sep}}{r_p} . \tag{1}$$

Inserting the synchrotron tunes $Q_{SPS} \approx 0.003$ or $Q_{LHC} \approx 0.006$, the circumferences $C_{SPS} \approx 6.9$ km or $C_{LHC} \approx 27$ km, the bunch spacing $L_{sep} \approx 7.5$ m, the chamber half apertures $(h_x h_y)_{SPS} \approx 1.3 \times 10^{-3}$ m$^2$ or $(h_x h_y)_{LHC} \approx 4 \times 10^{-4}$ m$^2$, the beta functions $\beta_{SPS} \approx 40$ m or $\beta_{LHC} \approx 100$ m, and the momenta $p_{SPS} \approx 26$ GeV/c or $p_{LHC} \approx 450$ GeV/c, we find a threshold bunch population of $N_{thr,SPS} \approx 4 \times 10^9$ for the SPS, and $N_{thr,LHC} \approx 1 \times 10^{11}$ for the LHC. Thus, the LHC beam is expected to be 25 times more stable vertically than the SPS beam, for the same electron line density. In the worst possible case, with strong multipacting all around the entire LHC circumference, the threshold will be reached close to the LHC design intensity. The actual threshold observed in the SPS is the threshold for multipacting and not the instability threshold for a saturated (or constant) electron cloud density calculated above.

Some uncertainties however remain. Direct simulations of the single-bunch instability in the LHC using the code HEADTAIL [7] yield the emittance growth rate as a function of electron density. The result is illustrated in Fig. 1. The emittance growth steeply increases with the electron density. However, even the smallest growth rates in Fig. 1 represent a significant emittance dilution over the time scale of the LHC injection plateau (20 minutes) or in collision (24 hours). It is peculiar that there is no threshold. The origin of the simulated emittance growth is presently under study, and it is further discussed in a companion paper [9].

## 3 VACUUM

While in the SPS the electron cloud manifests its presence by a large pressure increase [10], the situation may be the opposite in the warm sections of the LHC (about 20% of the circumference), where the vacuum chambers are coated by TiZrV getter, with a sticking coefficient of 1 for ions. The reason is that not only ionization by the beam can contribute to the pumping of the residual gas [11], but, more importantly, ionization by the low-energy electron. At saturation, the average number of electrons roughly equals that of the protons [12]. Then the linear pumping speed
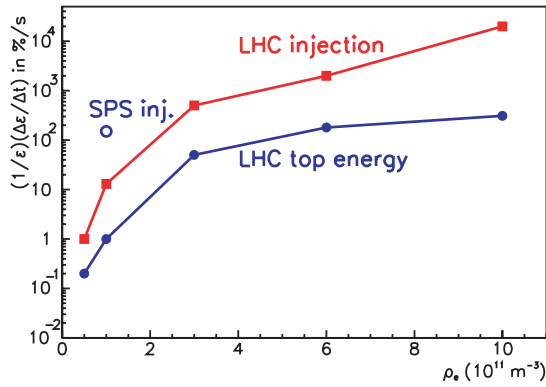
Figure 1: Simulated LHC emittance growth rates in %/s vs. average cloud density [8].

of the electron cloud is $S_{\mathrm{lin},e^-} \approx \sigma_e I_b/e$, where $I_b$ denotes the beam current and the ionization cross section $\sigma_e$ for the low-energy electrons is two orders of magnitude larger than that of the ultra-relativistic protons (100–400 Mbarn instead of 0.4–2 Mbarn). The estimated electron pumping is $S_{\mathrm{lin},e^-} \approx 20\,\mathrm{ls^{-1}m^{-1}A^{-1}}$ for $H_2$ and $130\,\mathrm{ls^{-1}m^{-1}A^{-1}}$ for methane, which will reduce the pressure.

## 4  BUILD UP AND HEAT LOAD

The build-up of an electron cloud along an LHC bunch train (batch) has been simulated using the ECLOUD code [13]. Results for different bunch intensities both in dipoles and field-free regions are displayed in Figs. 2 and 3. At first the electron density increases as a function of bunch intensity; it reaches a maximum for bunch intensities between about $8 \times 10^{10}$ and $10^{11}$; for even higher bunch intensities it decreases again. This non-monotonic dependence might be related to the 'lock-out' regime of S. Heifets [14].
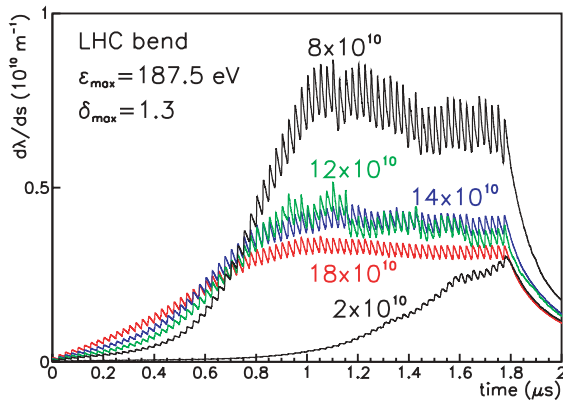


Figure 2: Electron line density as a function of time during the passage of a batch in an LHC dipole, for $\delta_{\max} = 1.3$, $\epsilon_{\max} = 187.5$ eV and different bunch intensities.

A firm commissioning constraint for the LHC is the heat load deposited on the cold bore of the arc chamber. Figure 4 shows the simulated average LHC arc heat load as a function of the bunch intensity for two different values of $\delta_{\max}$. Also indicated is the available cooling capacity, which decreases for higher intensities due to the enhanced heating by synchrotron radiation and image currents. For a maximum secondary emission yield $\delta_{\max} = 1.1$, the
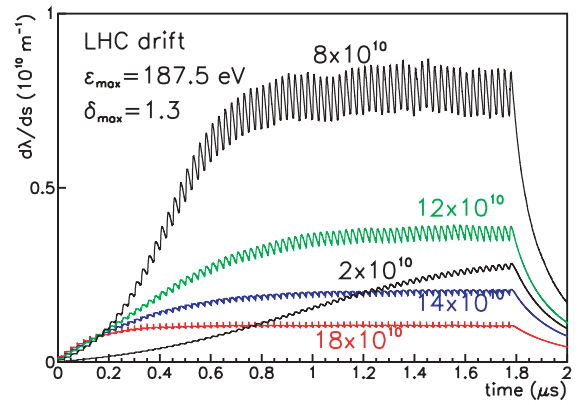


Figure 3: Electron line density as a function of time during a batch passage in an LHC field-free arc region, for $\delta_{\max} = 1.3$, $\epsilon_{\max} = 187.5$ eV and different bunch intensities.

threshold at which the simulated heat load surpasses the cooling capacity is equal to the ultimate LHC intensity of $N_b \approx 1.7 \times 10^{11}$. For $\delta_{\max} = 1.3$ the simulated threshold drops to $N_b \approx 5 \times 10^{10}$, about half the nominal design intensity. These numbers agree to within about 20% with earlier simulations [8].
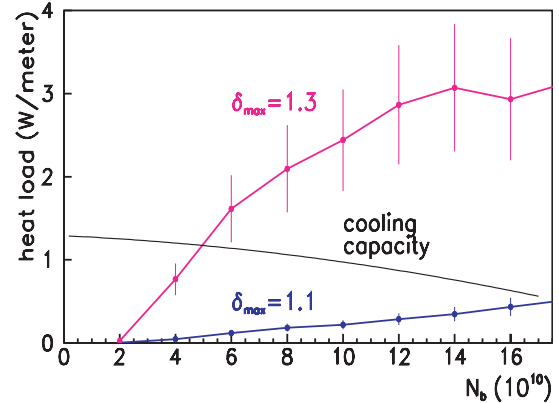


Figure 4: Average LHC arc heat load simulated in 2003 and cooling capacity as a function of bunch population $N_b$.

The exact modelling of the elastic electron reflection between 0 and 10 eV is still uncertain. Recent measurements [15] indicate that the probability of elastic reflection may approach 1 in the limit of 0 incident energy, while in our present parametrization this probability varies roughly between 0.2 and 0.6 depending on the value of $\delta_{\max}$. Modifying the low-energy reflectivity would increase the predicted heat load and could enlarge the simulated survival times.

## 5  SPS BENCHMARKS

In 2002, a discrepancy between the measured and simulated location of the electron-cloud stripes in a dipole field has been a major concern. The stripes occur in the region with maximum multipacting, and their position is sensitive to details of the secondary emission. After a revision of the ECLOUD code, we now obtain a satisfactory agreement, at the 10–15% level. A comparison of the measured [10] and newly simulated horizontal stripe position as a function of bunch intensity can be found in [8, 16]. Figure 5 unveils the

sensitivity of the electron position to rather small changes in the dipole magnetic field, and also the effect of changing the maximum secondary emission yield. The latter does not affect the position of the stripes, but alters the overall electron flux to the wall.
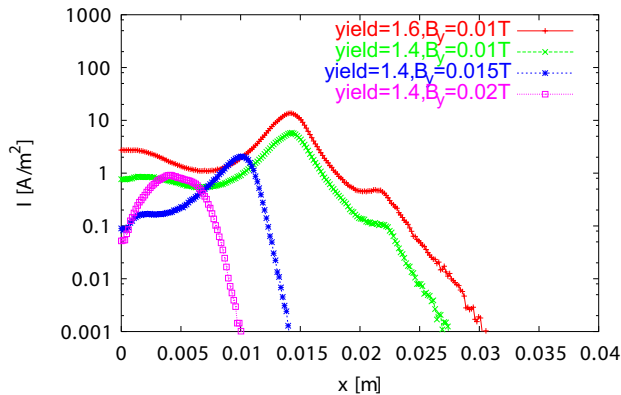


Figure 5: Simulated electron flux vs. horizontal position $x$ in the SPS for an intensity of $N_b = 1.2 \times 10^{11}$, two different magnetic fields and yields $\delta_{\max}$. The beam is at $x = 0$.

The simulated energy distribution of electrons impinging on the chamber wall is shown in Fig. 6. For a field of 100 G the distribution has a maximum at 200 eV, in good agreement with observations [10]. Simulated and measured energy spectra above 30 eV also agree well without magnetic field [8, 10]. Electrons at energies below 30 eV have not been measured and are not included in Fig. 6. However, in the simulation the overwhelming majority of the incident electrons are at these low energies.
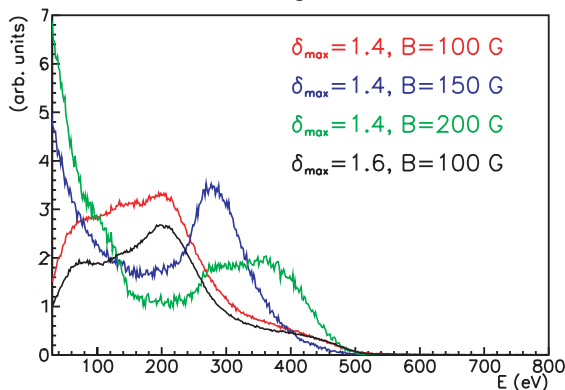


Figure 6: Simulated electron energy distribution at the wall for a dipole field in the SPS.

The measured and simulated absolute flux of electrons onto the chamber wall was compared, considering only the electrons of energy larger than 20 eV, for the passage of 1–3 batches [8]. For any number of batches, in a dipole field the measured flux is about 6 times lower than simulated. This difference may be due to the limited energy and momentum acceptance of the strip detector. In a 100-G field the cyclotron radius is $\rho \approx 750~\mu$m at 5 eV and 3.4 mm at 100 eV. These values are comparable to the chamber hole radius of 1 mm. Also the partial suppression of the cloud build up by the detector itself could contribute to the discrepancy. However, in the case without magnetic field the

difference between simulations and measurement is much larger, about a factor 35. This could indicate that we do not model the field-free case correctly.

For the successful commissioning of the LHC a reliable prediction of the heat load in the cold part of the machine is important. Several warm and cold calorimeters were installed in the SPS [17], whose purpose is to measure the actual heat load for different apertures, temperatures, and beam conditions. Their results serve as a benchmark for the simulations. Extensive measurements were performed for different numbers (1–4) of LHC batches. The measured heat loads [17] span a wide range, extending from 30 mW/m for 1 batch in a warm large-aperture calorimeter to 8 W/m for 3 batches in a cryogenic environment. Within the large scatter of the experimental data points, the measurements are consistent with the simulations for all the cases compared. However, the exact value of the secondary emission yield in the calorimeters is not precisely known and can rapidly change during beam operation, so that in some cases the experimental data fluctuate by a factor of 10. Measurements and simulations disagree on the effect of a magnetic field. The simulated heat load is maximum without field, while the observed one is two times higher at 100 G. Further benchmarking studies are planned for 2003.

## 6 CONCLUSIONS

Over the last three years an enormous progress has been made at CERN in electron-cloud diagnostics, beam measurements, and simulations. In general, the observations and simulations appear consistent. The successful suppression of the electron cloud in the SPS lends further confidence that we will be able to cure it in the more challenging environment of the LHC, with a cold vacuum system, a reduced clearing gap, and, at higher beam energies, a large number of primary photo-electrons from synchrotron radiation. Most open questions are under investigation.

## 7 REFERENCES

[1] O. Gröbner, Xth HEACC, Serpukhov (1977).

[2] G. Arduini, EPAC 2002, Paris, La Villette (2002).

[3] K. Cornelis, Proc. ECLOUD'02, CERN, Geneva, April 15-18, CERN-2002-001 (2002).

[4] K. Cornelis, CERN Mini-Workshop *http://sl.web.cern.ch/-SL/sli/Scrubbing-2002/Workshop.htm* (2002).

[5] F. Zimmermann et al., APAC'01, CERN SL-2001-057 (AP).

[6] K. Ohmi et al., PRL 85, p. 3831 (2000).

[7] G. Rumolo et al., SL-Note-2002-036 (2002).

[8] F. Zimmermann et al., Proc. Chamonix XII (2003).

[9] E. Benedetto et al., these proceedings.

[10] M.J. Jimenez, et al., Proc. Chamonix XII, 2003.

[11] C. Benvenuti, M. Hauer, ISR-VA/CB/sm (1976).

[12] A. Rossi et al., Proc. ECLOUD'02, CERN, Geneva, April 15-18, CERN-2002-001 (2002).

[13] G. Rumolo et al., SL-Note-2002-016 (AP) (2002).

[14] S. Heifets, Proc. ECLOUD'02, CERN, Geneva, April 15-18, CERN-2002-001 (2002).

[15] I. Collins, R. Cimino, private communication (2003).

[16] L. Evans, "Beam Physics at LHC," these proceedings.

[17] V. Baglin, B. Jenninger, CERN Mini-Workshop *http://sl.-web.cern.ch/SL/sli/Scrubbing-2002/Workshop.htm* (2002).